Scientific Article

Quantitative temporal diffusion spectroscopy as an early imaging biomarker of radiation therapeutic response in gliomas: A preclinical proof of concept

Xiaoyu Jiang PhD [a,b], Junzhong Xu PhD [a,b,c,d,e], John C. Gore PhD [a,b,c,d,e,f,]*

[a]Institute of Imaging Science, [b]Department of Radiology and Radiological Sciences, [c]Vanderbilt-Ingram Cancer Center, [d]Department of Physics and Astronomy, [e]Department of Biomedical Engineering, and [f]Department of Molecular Physiology and Biophysics, Vanderbilt University, Nashville, Tennessee

Abstract

Purpose: This study aims to test the ability of quantitative temporal diffusion spectroscopy (qTDS) to assess cellular changes associated with radiation-induced cell death in a rat glioma model.

Methods and Materials: Tumor response to a single fraction of 20 Gy of x-ray radiation was investigated in a rat glioma (9L) model. Tumor response was monitored longitudinally at post-inoculation days 21, 23, and 25, using a specific implementation of qTDS with acronym IMPULSED (Imaging Microstructural Parameters Using Limited Spectrally Edited Diffusion), as well as conventional diffusion and high-resolution anatomic imaging. IMPULSED method combines diffusion-weighted signals acquired over a range of diffusion times that are then analyzed and interpreted using a theoretical model of water diffusion in tissues, which generates parametric maps depicting cellular and subcellular structural information on a voxel-wise basis. Results from different metrics were compared statistically.

Results: A single dose of 20 Gy x-ray radiation significantly prolonged survival of 9L-bearing rats. The mean cell sizes of irradiated tumors decreased ($P < .005$) after radiation treatment, which we associate with cell shrinkage and the formation of small cellular bodies during apoptosis and necrosis. A combination of IMPULSED-derived parameters (mean cell size d and extracellular structural parameter β_{ex}) separated 90% of irradiated tumors from the nonirradiated cases at post inoculation day 23, whereas a combination of tumor growth and conventional apparent diffusion coefficient did not differentiate irradiated tumors from nonirradiated tumors.

Conclusions: This proof-of-concept study demonstrates the IMPULSED method to be a new method for deriving quantitative microstructural parameters in a preclinical tumor model. The method provides unique information based on the diffusion time dependency of diffusion magnetic resonance imaging, which cannot be obtained by conventional diffusion weighted imaging methods, and the results have a close correlation with primary biologic markers of treatment efficacy, such as cell death and survival.

Introduction

The successful treatment of malignant brain tumors remains one of the most challenging problems in oncology despite advances in systemic therapies, including surgery, radiation therapy (RT), and chemotherapy. A central question is whether individual tumors are responding positively. Currently, measuring tumor shrinkage is the gold standard clinical imaging criterion for evaluating the response of solid tumors.[1,2] However, changes in tumor volume can be reliably detected only in late stages of treatment (usually 2-3 months after starting treatment) and may not be a reliable indicator of tumor response and/or patient prognosis.[3] The availability of earlier and more accurate predictive indicators of treatment response would be of obvious benefit to individual patients and in advancing the treatment of brain tumors more generally by facilitating clinical trials of new approaches.

Diffusion-weighted magnetic resonance (MR) imaging (DWI) has been previously exploited as a potential imaging approach for assessing microstructural changes that occur early in a treatment course.[4,5] The clinical use of DWI relies on the observation that it often provides an indirect measurement of cellularity because values of the apparent diffusion coefficient (ADC) decrease as cells pack more densely during proliferation. DWI has been found to be able to predict early radiation response in brain tumors[6] by assessing treatment-induced cell loss before tumor shrinkage. Conventional DWI measures MR signal decreases caused by water diffusion using a single, relatively long, diffusion time. However, the ADC derived from measurements using a single diffusion time is potentially affected by multiple biophysical properties other than cellularity,[7] including cell size,[8] nuclear size,[9] membrane permeability,[10] and the presence of necrosis.[11] It also depends on the choices of scanning parameters (eg, gradient amplitudes and duration). These confounding factors prevent accurate interpretation of ADC and ultimately limit the clinical use of single-ADC measurements for assessing treatment response.

To overcome the shortcomings of conventional DWI methods, quantitative temporal diffusion spectroscopy (qTDS) has been developed. It incorporates 2 significant modifications.[12–17] First, by including oscillating diffusion gradients other than conventional unipolar gradients, the ADC may be measured at very short diffusion times, before water molecules have moved very far, allowing the detection of subcellular structural changes.[9,18,19] Second, by measuring the dependence of ADC on the diffusion time over a range of times, several cellular properties, such as cell sizes, may be separately derived. Recently we described a specific implementation of qTDS with acronym IMPULSED (Imaging Microstructural Parameters Using Limited Spectrally Edited Diffusion) that combines acquisitions over a range of gradient waveforms and frequencies that cover a specific range of different diffusion times, which, in combination with a biophysical model of diffusion in cellular tissues, allows reliable measurements of tissue microstructure over length scales of microns, characteristic of cancer cell sizes and smaller. IMPULSED has been found to accurately quantify cell sizes in vitro for different cancer cell types at varying cell densities, as well as a breast cancer cell line before and after antimitotic treatment.[14] IMPULSED has also provided maps of cell size and cell densities in vivo for 3 types of human colon cancer that agreed strongly with histologic analysis.[20] In addition, qTDS has been reported to be capable of detecting cell swelling during mitotic arrest induced by cytotoxic treatments in animal models[21] and cell shrinkage during chemotherapy-induced apoptosis.[22] We hypothesized that IMPULSED method has sufficient sensitivity and specificity to quantify RT-induced changes in specific cellular properties that occur earlier than tumor regression and thus could provide more reliable early indicators of treatment response. In this study the response to radiation treatments of a rat glioma model was monitored longitudinally using IMPULSED and other MR imaging (MRI), including standard DWI measurements of ADC. Results from different metrics were statistically compared.

Methods and Materials

Animal model and radiation treatment

All experiments were performed in a 9L glioma rat model, with all animal procedures approved by the Institutional Animal Care and Usage Committee. Male Sprague-Dawley rats were used for the study and observed daily and weighed weekly to ensure that interventions were well tolerated.

The 9L tumor-bearing rats were irradiated with an orthovoltage x-ray unit (Pantek 300 DXT, Branford, CT). Each irradiated rat was shielded to expose only the portion of the brain that contains the tumor to a single

fraction of 20 Gy radiation. Rats were anesthetized with a 2%/98% isoflurane/oxygen mixture during irradiation. The 20 Gy irradiation lasted about 10 minutes.

Experimental outline

Two sets of experiments, a long-term survival experiment and a short-term treatment response imaging study, were performed. For the survival experiment, 16 tumor-bearing rats were randomly divided into a nonirradiated group (n = 8) and an irradiated group (n = 8). Rats were sacrificed if they lost more than 20% body weight or suffered obvious behavioral detriments (eg, ataxia) or at 45 days after tumor cell inoculation. For the treatment response imaging study, 18 tumor-bearing rats were divided into a nonirradiated group (n = 9) and an irradiated group (n = 9). Tumors were similarly implanted and tumor size and location were confirmed by MRI at postinoculation day (PInD) 21. All the rats were imaged on PInD 21, 23, and 25. The irradiated group received RT (20 Gy, single fraction) on PInD 21 immediately after the first imaging session. Immediately after the last imaging session, all rats were sacrificed using intracardiac perfusion with 0.1 mol/L phosphate-buffered saline and formalin. The rats were then decapitated, and heads were immersed in formalin for 24 hours and processed for paraffin sectioning and subsequent hematoxylin and eosin (H&E) staining. Nuclei size distribution was obtained from digitized H&E-stained images using in-house MAT-LAB code (Mathworks, Natick, MA).

In vivo MRI

Rats were anesthetized with a 2%/98% isoflurane/oxygen mixture before and during scanning. All images were acquired with a Varian DirectDrive horizontal 9.4 T magnet (Varian Inc, Palo Alto, CA). The magnet bore temperature was kept at 32°C using a warm-air feedback system. Rats were restrained during imaging in a customized Teflon animal holder with a tooth bar and a head bar.

Diffusion-weighted imaging sequences were implemented using a 2-shot spin-echo echo planar imaging acquisition. A conventional pulsed gradient spin echo (PGSE) sequence acquired data using pairs of unipolar diffusion gradients of duration δ = 4 ms and separation Δ = 48 ms. Shorter diffusion times were achieved using pairs of oscillating gradients (OGSE) with gradient frequencies from 50 to 150 Hz with δ/Δ = 20/25 ms, corresponding to effective diffusion times (1/4f, where f is the frequency[23]) from approximately 5 to 1.7 ms. Five gradient (b) factor values spaced at equal logarithmic intervals from 0 to either 2000 s/mm^2 or the allowed maximum b value (limited by our maximum gradient strength of 360 mT/m in a single direction) were used for both PGSE and OGSE acquisitions. Multiple axial slices covering the entire tumor of each animal were acquired with a slice thickness of 2 mm. The matrix size was 96 × 96 with field of view = 32 × 32 mm, yielding an in-plane resolution of 333 × 333 μm^2. Note that the echo times (TE = 67 ms) were the same for all diffusion measurements to minimize differential relaxation effects.

qTDS diffusion model

The diffusion-weighted signals of tumor tissues can be expressed as the sum of signals arising from the intra- and extracellular spaces:

$$S = v_{in} \times S_{in} + (1 - v_{in}) \times S_{ex} \qquad (1)$$

where v_{in} is the water volume fraction of intracellular space and S_{in} and S_{ex} are the diffusion weighted signal magnitudes per volume from the intra- and extracellular spaces, respectively. This analysis assumes the effects of water exchange between intra- and extracellular spaces during the diffusion time are negligible, as suggested in previous models of diffusion in tumors[13,14] and which is especially justifiable for short diffusion times.[24] Tissue is considered to be composed of packed spherical cells of dimension d, although this parameter is more appropriately interpreted as the average dimension characterizing restrictions to free diffusion of the intracellular water. Analytical expressions of S_{in} and S_{ex} acquired by OGSE and PGSE sequences have been reported previously[15] and are summarized in the following equations (Eq. 2-5):

$$S_{in}(OGSE) = \exp\left(-2(\gamma g)^2 \sum_n \frac{B_n \lambda_n^2 D_{in}^2}{(\lambda_n^2 D_{in}^2 + 4\pi^2 f^2)^2} \right.$$
$$\left\{ \frac{(\lambda_n^2 D_{in}^2 + 4\pi^2 f^2)}{\lambda_n D_{in}} \left[\frac{\delta}{2} + \frac{\sin(4\pi f \delta)}{8\pi f} \right] - 1 \right.$$
$$+ exp(-\lambda_n D_{in}\delta) + \exp(-\lambda_n D_{in}\Delta) \qquad (2)$$
$$\left. \left. (1 - \cosh(\lambda_n D_{in}\delta)) \right\} \right)$$

$$S_{in}(PGSE) = \exp\left(-2\left(\frac{\gamma g}{D_{in}}\right)^2 \sum_n \frac{B_n}{\lambda_n^2} \{ \lambda_n D_{in}\delta - 1 \right.$$
$$+ \exp(-\lambda_n D_{in}\delta) + \exp(-\lambda_n D_{in}\Delta) \qquad (3)$$
$$\left. (1 - \cosh(\lambda_n D_{in}\delta)) \} \right)$$

$$S_{ex}(OGSE) = \exp[-b(D_{ex0} + \beta_{ex} \cdot f)] \qquad (4)$$

$$S_{ex}(PGSE) = \exp[-bD_{ex0}] \qquad (5)$$

where D_{in} is the intracellular diffusion coefficient, f is the oscillation frequency, δ is the gradient duration, Δ is the separation of 2 diffusion gradients, g is the gradient

amplitude, and λ_n and B_n are structure-dependent parameters that depend on the spherical cell diameter d, D_{ex0} is the extracellular diffusion rate at frequencies close to 0, and β_{ex} is the slope of extracellular diffusion coefficient with respect to frequency f, which also contains information on structural dimensions. Explicit expressions for λ_n and B_n have been reported previously.[15] Note the effective diffusion time for OGSE is 1/4f.[23] Five parameters (cell size d, intracellular diffusion coefficient D_{in}, intracellular volume fraction v_{in}, and extracellular parameters D_{ex0} and β_{ex}) can then be estimated by fitting to the measured data.

Data analysis and statistics

Data sets were analyzed using purpose-written MATLAB programs. IMPULSED method extracts the 5 quantities that describe diffusion in tissue from measurements of the dependence of ADC on gradient frequency or diffusion time. The effective diffusion time range used in IMPULSED determines what structural length scales can be explored. In this study, effective diffusion times ranging from 1.7 to 48 ms were used to sensitize the data to glioma cells, whose sizes are about 5 to 15 μm. For comparison, the mean square displacement of water molecules in 1 direction with intrinsic diffusion coefficient of 3×10^{-5} cm^2/s^{-1} by Einstein's diffusion equation is 3 to 17 μm for this range of diffusion times. By contrast, the ADC values of normal brain tissues and necrotic/late apoptotic regions stay relatively constant within this diffusion time range, either because the structural length scale is too short to affect measured values of ADC or because there are so few intact cells that restriction effects are not appreciable. Therefore each voxel within the tumor-bearing rat brain first went through a Bayesian-based model selection process[25] to determine which diffusion model (either constant ADCs at different diffusion times/oscillating gradient frequencies or the qTDS model) is statistically more justified. For voxels to be fit using IMPULSED model, the 5 unknown variables were estimated using the lsqcurvefit function in MATLAB. The constraints for fitting parameters were based on physiologically relevant values[14,26,27]: $0 \leq d \leq 40$ μm; $0 \leq v_{in} \leq 1$; $0 \leq D_{in} \leq 3.0$ μm^2/ms; $0 \leq D_{ex0} \leq 3.0$ μm^2/ms; and $0 \leq \beta_{ex} \leq 10$ μm^2. Randomly generated initial parameter values were used in the fittings.

The mean values of each metric across IMPULSED-defined regions of interest (ROIs) were calculated to compare irradiated and nonirradiated groups. The temporal behavior differences in IMPULSED-derived parameters, T2-weighted (T2W) image−derived tumor volumes, and conventional ADC values between nonirradiated and irradiated 9L-bearing rats were summarized using mean and standard error of mean and compared by
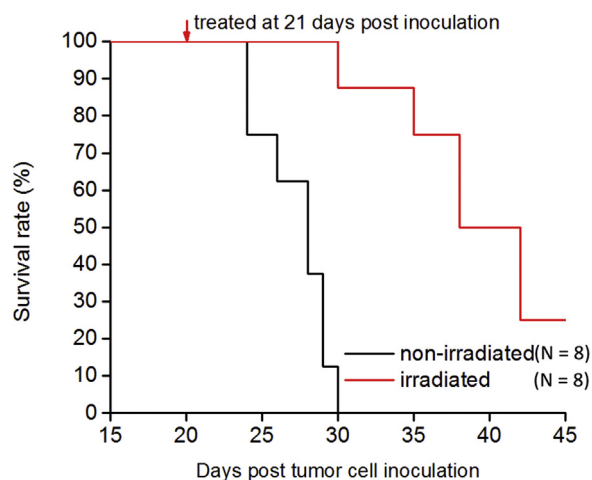
Figure 1 Survival rates for irradiated (red) and nonirradiated (black) 9L-bearing rats. The radiation therapy was given on postinoculation day 21.

repeated measures 2-way analysis of variance with Holm-Bonferroni posttests.

Results

Survival data are shown in Figure 1 for irradiated and nonirradiated groups. A single dose of 20-Gy x-ray radiation given 21 days after inoculation of tumor cells led to a significant increase in median survival compared with nonirradiated controls ($P = .0024$).

Figure 2 shows that the rate of signal decay with increasing gradient b factor depends on the frequency of the gradient encoding used in the acquisition. The slopes of the decays correspond to ADC values at different diffusion times, and they increase with increasing gradient frequency (decreasing diffusion time), consistent with a model in which restricting boundaries affect water movements less when the molecular displacements in the time of the measurement are smaller than the scale of the restrictions.

Figure 3 shows a T2-weighted image, a conventional ADC map, and IMPULSED-derived parametric maps and corresponding H&E images for a representative slice from a nonirradiated rat. Each of the parametric maps shows regional heterogeneity that is not the same for each property. The pattern of the conventional ADC map is consistent with the H&E images. Necrotic core regions (ROI 3) and peritumoral edema (ROI 4) have very high ADCs. ROI 2 with excess cytologic atypia and numerous mitoses (Fig 3A-b) has moderately high ADCs, whereas regions with less atypia (Fig 3A-a) have very low ADCs. Conventional ADCs are sensitive to variations in cell density but lack specificity. For example, ROI 2 has very similar ADCs with the contralateral normal side.
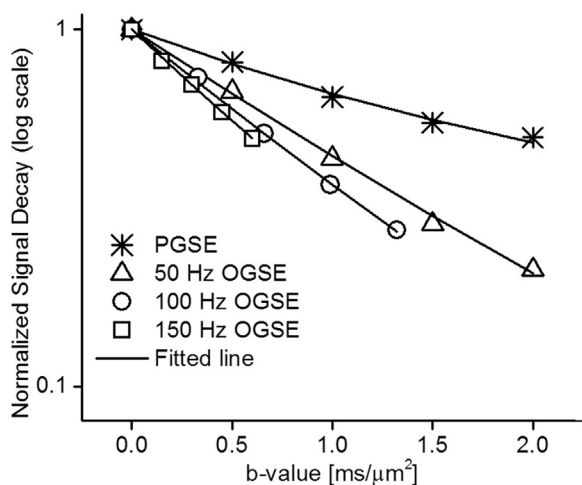
Figure 2 Typical oscillating gradient spin echo (OGSE) (50, 100, and 150 Hz) and pulsed gradient spin echo (PGSE) single-voxel signals for voxels from a 9L tumor. The solid line represents the fit using IMPULSED model.

As mentioned previously, a voxel-based model selection between the constant ADC and IMPULSED models can differentiate regions of viable tumor cells from regions of late-stage apoptotic/necrotic cells. The voxels that favor the qTDS model correspond to the IMPULSED-derived region shown in Figure 3D. This region excludes normal brain tissue, edema, and a necrotic core and matches the tumor shape found in histology in general, despite the significant distortion and tissue shrinkage displayed on H&E image.

Figures 3E, F, H, I, and J show the 5 IMPULSED-derived parameters that describe the tumor microstructure. The IMPULSED-derived mean cell size of 9L tumor is $\sim 12\ \mu m$. Maps of D_{ex0} (Fig 3H) show spatial patterns very similar to those of conventional ADC maps, indicating they both reflect the diffusion rate in the extracellular space. The other 4 parametric maps are very different from conventional ADC maps, suggesting that qTDS provides more comprehensive information to describe the tumor microstructure.

Figure 4 shows T2W anatomic images and histograms of IMPULSED-derived parameters and conventional ADC of exemplar 9L-bearing nonirradiated (A and C) and irradiated (B and D) animals at baseline (PInD 21) and at later time points (PInD 23 and 25). For the T2W images, different columns represent 3 contiguous slides from the same animal. Slides with the same anatomic characteristics were chosen for different time points. Visual comparison of the size of tumors (Fig 4A, B) reveals that the tumor growth of irradiated 9L tumor was mediated from PInD 23 to PInD 25 compared with nonirradiated tumor. For the irradiated tumor, there are evident shifts in both mean cell size and β_{ex} peaks toward lower values during tumor progression (Fig 4D-a, D-e), whereas distributions of mean cell size and β_{ex} are almost the same across all time points for the nonirradiated tumor (Fig 4C-a, C-e).

The treated tumor shows a clearly visible increase in conventional ADC from PInD 21 to 25 (Fig 4D-f). However, conventional ADC of the nonirradiated tumor also shows a dramatic increase from PInD 23 to 25 (Fig 4C-f), making reliable detection of treatment effects difficult.

Figure 5A and 5E shows the progression of the mean tumor volumes from T2W and diffusion images along with IMPULSED-derived parameters for nonirradiated and irradiated rats. Irradiated rats had a greatly diminished volume of tumor at PInD 25 compared with nonirradiated controls ($P = .0055$), indicating a strong mitigative effect as a result of radiation.

The conventional ADC values for irradiated tumors increased after RT ($P = .0088$), consistent with RT-induced cell loss. However, conventional ADC values for the nonirradiated tumors also had an increasing trend for PInD 23 to PInD 25. The differences in conventional ADC values between irradiated and nonirradiated tumors were not significant at any of the imaging time points.

The mean cell sizes of irradiated tumors decreased ($P = .0044$) after RT, whereas those of nonirradiated controls increased from PInD 21 to PInD 23 ($P = .0329$), consistent with increased cell proliferation.[28] D_{ex0} had a trend similar to that of conventional ADC. β_{ex} detected the effects of treatment earlier than did conventional ADC. The detailed P values of multicomparison (Holm-Bonferroni) testing for differences in T2W-derived tumor volumes, conventional ADC, and IMPULSED-derived parameters between (1) nonirradiated and irradiated tumors and (2) baseline (PInD 21) and later time points (PInD 23 and 25) are reported in Table E1 (available online at https://dx.doi.org/10.1016/j.adro.2018.11.003). The biologic mechanisms behind these findings are discussed later.

Figure 6 is a scatter plot of the ratios of different metrics at PInD 23 and PInD 21 (conventional PGSE ADC vs T2W-derived tumor volume, β_{ex} vs mean cell size) for all animals. Figure 6A shows that the combination of the PInD 23/PInD 21 ratio of tumor volume and conventional ADC cannot differentiate irradiated tumors from nonirradiated tumors. By contrast, a square region defined by a PInD 23/PInD 21 ratio of $0 < \beta_{ex} < 1$ and $0 < $ mean cell size < 1 separate 8 of 9 irradiated tumors from all the nonirradiated cases (Fig 6B), suggesting the combination of IMPULSED-derived mean cell size and β_{ex} as an early indicator of radiation response. This criterion corresponds to cells shrinking after treatment, creating larger extracellular spaces whose effects on diffusion have less dependence on diffusion time.

Discussion

Temporal diffusion spectroscopy makes use of the variation of measured diffusion rates of water with
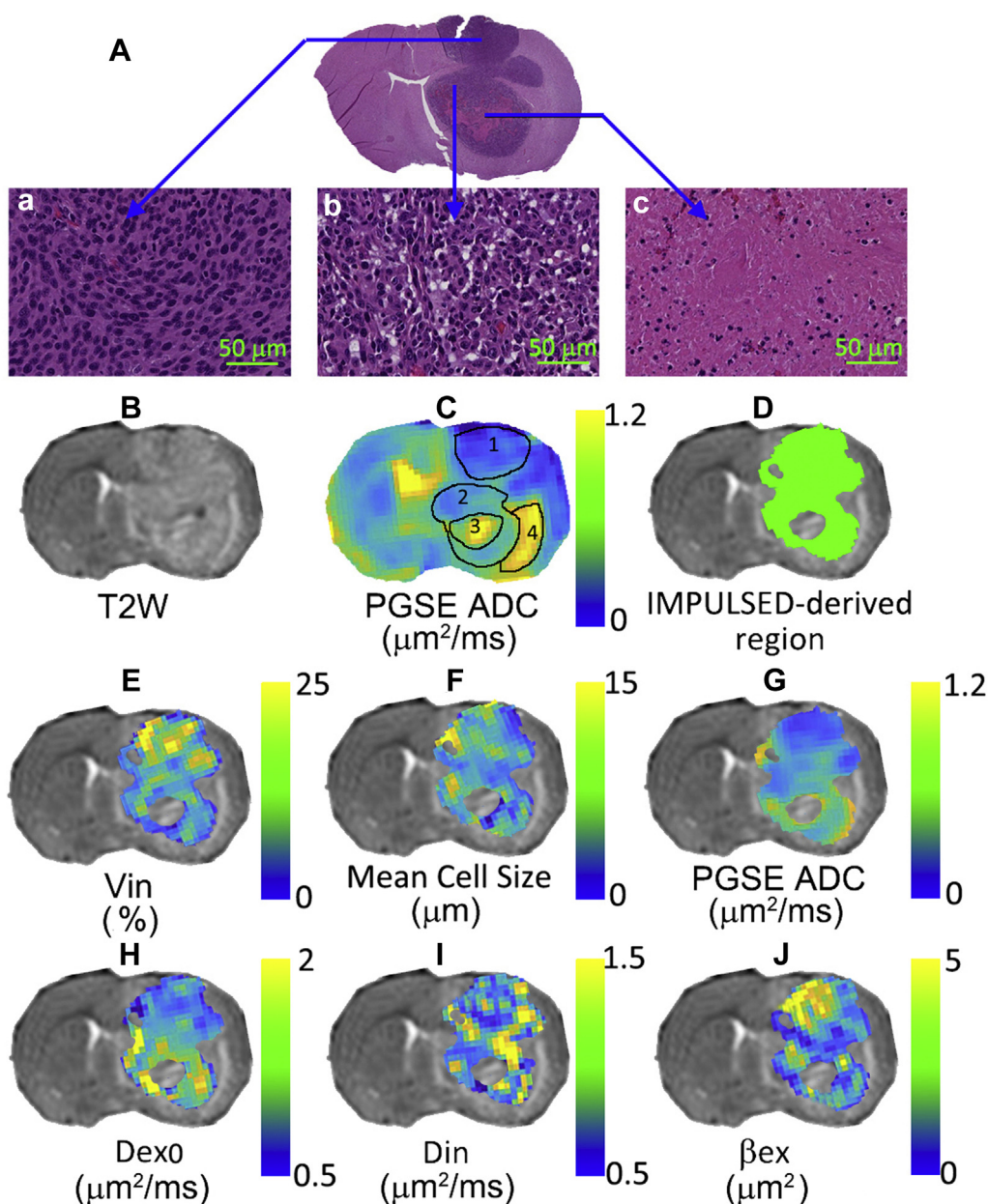
Figure 3   (A) Hematoxylin-eosin images, (B) T2-weighted (T2W) images, (C) conventional apparent diffusion coefficient (ADC) map, and (D-J) parametric maps derived by IMPULSED method overlapped on a T2W image of 9L tumor-bearing rat brain. Note IMPULSED-derived region excludes the necrotic/late-stage apoptotic and edema regions and thus provides an accurate segmentation of the actively growing tumor region. *Abbreviations:* βex = slope of extracellular diffusion coefficient; Dex0 = extracellular diffusion rate at frequencies close to 0; Din = intracellular diffusion coefficient; PGSE = pulsed gradient spin echo; Vin = water volume fraction of intracellular space.

diffusion time to derive information on the spatial scales of tissue structures. Building on the success of (1) mapping of cell size and cellularity in vitro and in vivo for different cancer cell types using qTDS[14,20,24] and (2) assessing cell size changes associated with treatment-induced cell cycle arrest[21] and apoptosis,[22] we investigated the value of qTDS for early detection of tumor response to RT in this study. As shown in Figure 3, the IMPULSED-derived mean cell size of 9L tumor at the last

imaging session was ∼12 μm, which is consistent with values in the literature.[27] In addition, the mean nuclei size calculated from the corresponding H&E-stained image is ∼8 μm (Fig. E1; available online at https://dx.doi.org/1 0.1016/j.adro.2018.11.003). The resulting nuclear/cyto-plasmic ratio is ∼1:2.3, which is reasonable according to previous literature.[29]

Currently, tumor response to radiation is assessed by monitoring tumor growth. Conventional DWI has also
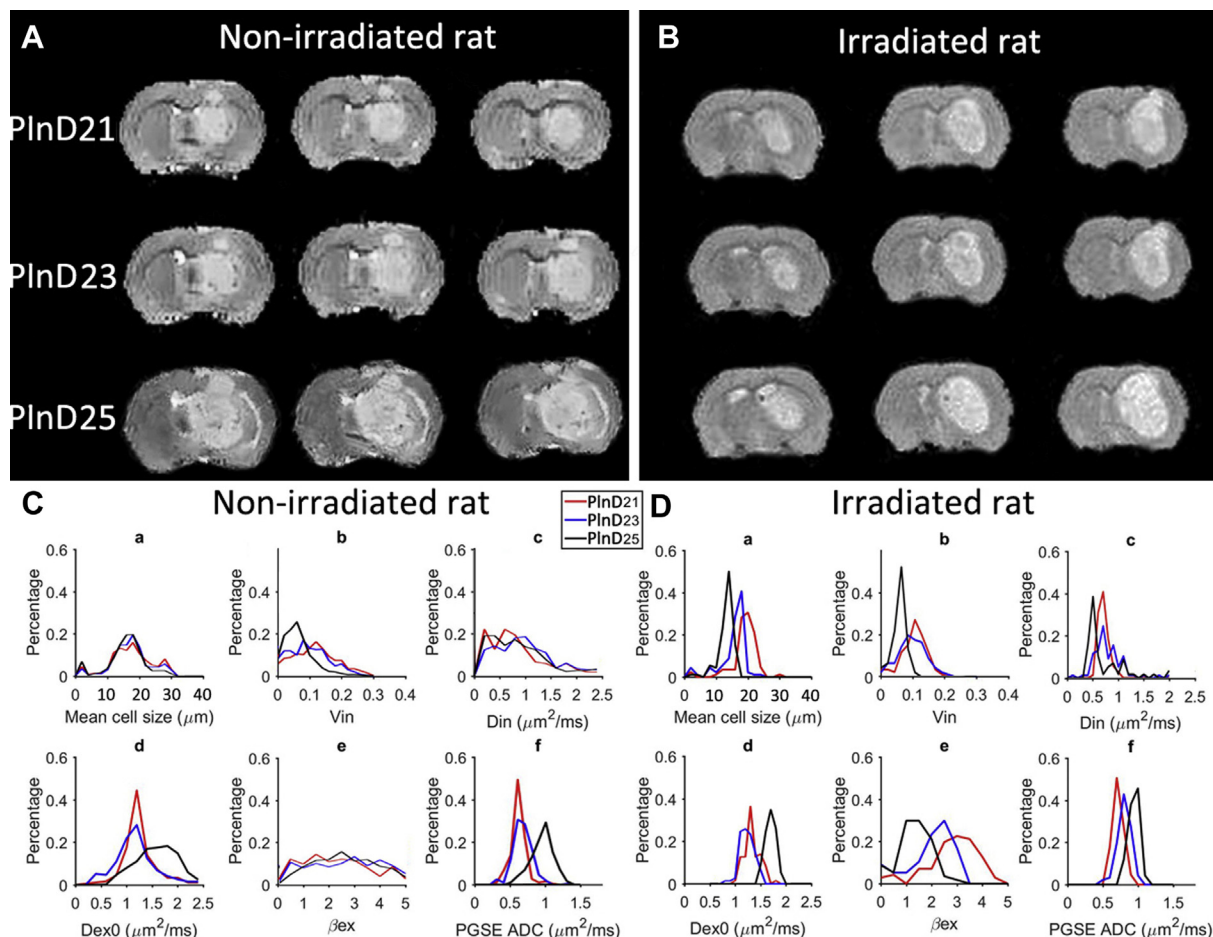
Figure 4   T2-weighted anatomic images and histograms of IMPULSED—derived parameters and conventional apparent diffusion coefficient (ADC) values from typical nonirradiated (A and C) and irradiated (B and D) animals at PInD 21, 23, and 25. *Abbreviations:* βex = slope of extracellular diffusion coefficient; Dex0 = extracellular diffusion rate at frequencies close to 0; Din = intracellular diffusion coefficient; PGSE = pulsed gradient spin echo; PInD = postinoculation day; Vin = water volume fraction of intracellular space.

been widely used to detect RT effectiveness, assuming that ADC measured with a relatively long diffusion time is inversely correlated with cell density. In this study we evaluated the performance of different imaging indicators (tumor volume, conventional ADC, mean cell size, and β_{ex}) for differentiating irradiated tumors from nonirradiated tumors at an early imaging time point (PInD 23). As shown in Figure 6, a square region defined by a PInD 23/PInD 21 ratio of $0 < \beta_{ex} < 1$ and $0 <$ mean cell size < 1 separate 8 out of 9 irradiated tumors from all the nonirradiated cases, whereas the combination of tumor volume and conventional ADC cannot differentiate irradiated tumors from nonirradiated tumors. This indicates that IMPULSED method, which is readily implemented on MR scanners, has significant potential to improve monitoring of radiation response in primary brain tumors. To the best of our knowledge, this is the first study to investigate the value of diffusion time dependency of diffusion MRI to assess tumor response to radiation.

Our preclinical data indicate that IMPULSED-derived parameters can detect radiation response earlier than can monitoring changes in tumor volume. Specific biological mechanisms that may account for this observation. Ionizing radiation may induce various processes (eg, mitotic-linked death, necrosis, autophagy, apoptosis, and senescence) in brain tumors that cause changes earlier than significant cell loss and tumor volume regression.[30-32] Although irradiated tumor cells enter different terminal pathways early after treatment, they eventually die through apoptosis or necrosis.[33-35] Cellular death caused by necrosis results in the loss of cell membrane integrity and an uncontrolled release of cellular contents into the extracellular space.[36] Apoptosis is characterized by a series of typical morphologic features, such as shrinkage of the cell, fragmentation into membrane-bound apoptotic bodies, and rapid phagocytosis by neighboring cells.[37] These changes decrease the length scales of the restrictions that hinder or restrict
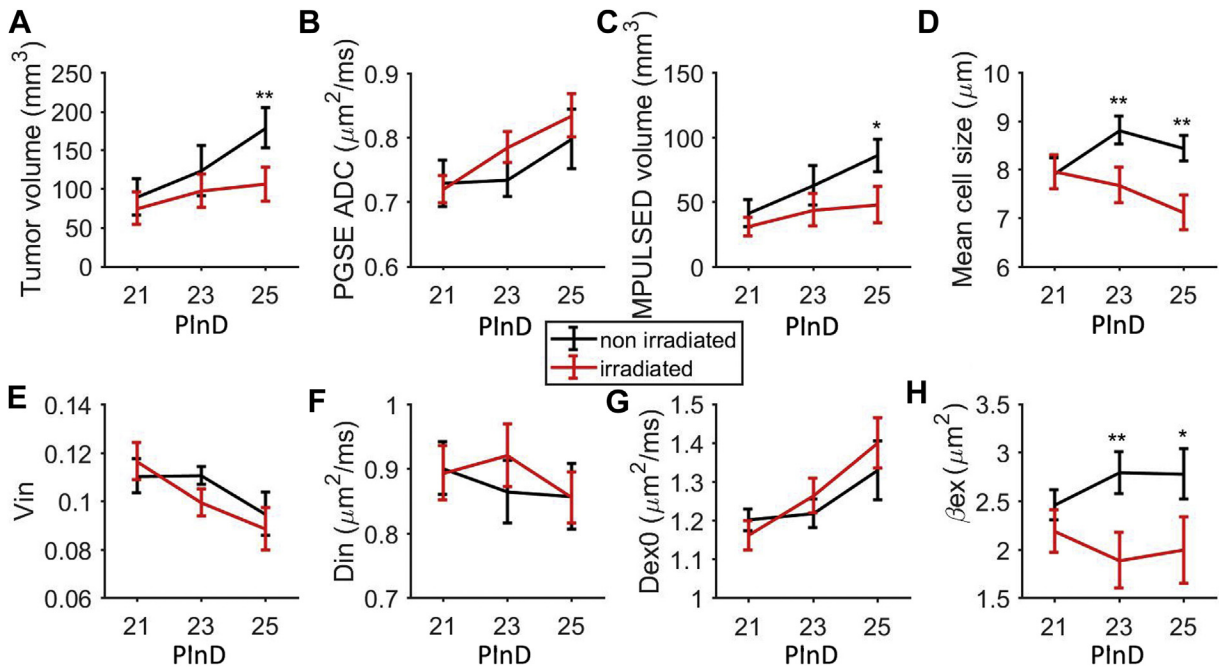
Figure 5   Temporal changes (mean ± standard error of mean, n = 9) in tumor volume measured by T2-weighted images, conventional apparent diffusion coefficient, IMPULSED−derived volume, and our in-house qTDS-derived parameters for irradiated and nonirradiated rats. *$P < .05$ and **$P < .01$, as measured by 2-way repeated-measures analysis of variance with a Holm-Bonferroni posttest. *Abbreviations:* βex = slope of extracellular diffusion coefficient; Dex0 = extracellular diffusion rate at frequencies close to 0; Din = intracellular diffusion coefficient; PInD = postinoculation day; Vin = water volume fraction of intracellular space.

tissue water movement, which may lead to a decreasing average cell size measured by IMPULSED. Because IMPULSED method emphasizes restrictions of a certain size range (depending on what diffusion times are used), very small apoptotic bodies and fragments of cellular debris cannot be further distinguished. There follows a decrease in the intracellular volume fraction and

decreasing tortuosity in the extracellular space, which in turn indicates lower dependence on diffusion time. IMPULSED can thus serve as an early biomarker of radiation-induced cell death.

We also found that ADCs obtained using a conventional DWI protocol did not differentiate irradiated tumors from nonirradiated tumors. In a conventional DWI
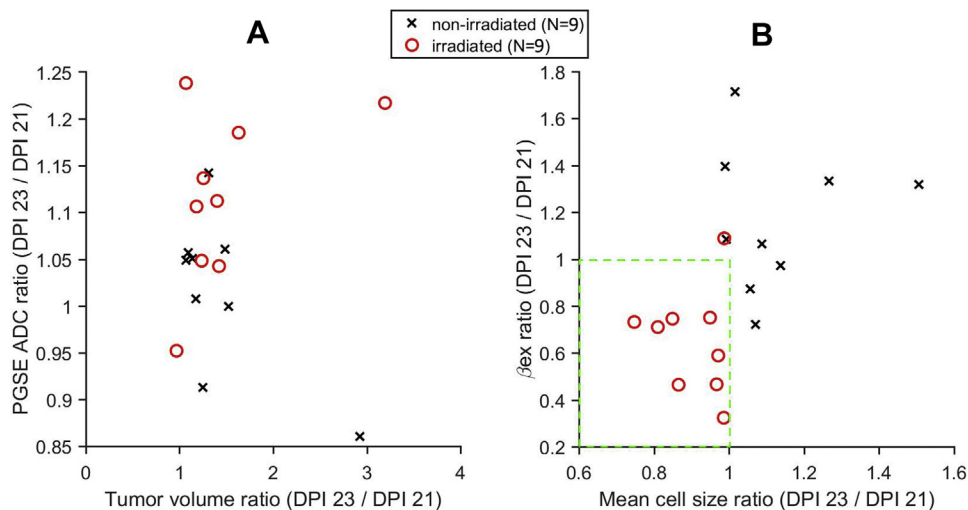
Figure 6   Scatter plot of the ratios of different metrics (conventional ADC/PGSE ADC, T2W-derived tumor volume, βex, and mean cell size) at PInD 23 to those at PInD 21. *Abbreviations:* β_{ex} = slope of extracellular diffusion coefficient; ADC = apparent diffusion coefficient; PGSE = pulsed gradient spin echo; PInD = postinoculation day; T2W = T2 weighted.

protocol, ADCs are usually correlated with cellularity. Although ADCs for irradiated rats kept increasing after RT, ADCs for nonirradiated rats also started to increase from PInD 23, likely because of the formation of necrotic cores in the growth of tumors. Therefore conventional ADC did not provide sufficient sensitivity or specificity for assessing radiation treatment responses in this model.

IMPULSED method may be adapted and translated for clinical applications, though the precise preclinical protocol used here cannot be applied on current clinical scanners. The oscillating gradients are readily implemented on clinical scanners, but the frequency range is limited by the available gradient strengths, which in practice imposes a limit around 80 Hz. However, the range up to 50 Hz is still of considerable relevance because it corresponds to a range of effective diffusion times (from 5 ms up) that still covers the typical length scales of many internal and external structures in tissues (≈ 5 microns and larger). We have implemented our in-house qTDS method on a Philips Achieva 3T scanner using a gradient strength < 60 mT/m and slew rate < 100 mT/m/s, which is commonly achievable for state-of-the-art clinical scanners.[38]

In this study the mean values of IMPULSED-derived parameters over tumor ROIs were used to assess tumor response. Other novel analyses of heterogeneity (eg, functional diffusion maps and ADC histograms,[6,39,40] texture analysis,[41] and radiomics approaches[42]) have been shown to add value for tumor staging, classification, and treatment response assessment. Our parametric maps and histograms indicate significant heterogeneity across tumor regions (Figs 3 and 4). This variation was not investigated in detail in this study because our primary goal here is to explore the advantages of a new method, IMPULSED, over standard clinical DWI methods for longitudinal RT response detection. A detailed exploration of local variations of IMPULSED-derived parameters (eg, combinations of IMPULSED and texture analysis) is ongoing and will allow more insights into the biophysical basis of IMPULSED results.

This study aims to test the ability of IMPULSED method to assess cellular changes associated with radiation-induced cell death. For this purpose, we chose a radiosurgery-like high-dose single-fraction irradiation to reliably trigger cell death of cancer cells and efficiently reverse or mitigate tumor growth. The results of the present study indicate that IMPULSED can serve as an early biomarker of radiation-induced cell death. Future studies will include assessing tumor response to fractionated radiation, which will improve the likelihood of translating IMPULSED method to current standard-of-care radiation treatments.

The effects of microcirculatory perfusion of blood within capillaries on ADC values were assumed to be negligible in the present study. This assumption has been made in previous treatment studies using DWI[10] because the perfusion fraction of tissues is usually much smaller than the diffusion fraction of tissues. In cases in which the effects of tumor angiogenesis on ADC measurements cannot be assumed to be negligible, ADC values can be calculated from diffusion-weighted signals acquired at only higher b values (>200 s/mm^2) that are not affected by perfusion, or the current PGSE/OGSE sequences can be modified to acquire perfusion-free MR signals by inserting a PGSE filter with a small b value at the beginning of each sequence.[11]

Conclusions

This proof-of-concept study has validated IMPULSED method for deriving quantitative microstructural parameters in a preclinical tumor model. Although this approach should be further examined in additional tumor models, we have described the power of using IMPULSED as a biomarker for the early detection of radiation treatment response in the 9L glioma model. The method provides unique information based on the diffusion time dependency of diffusion MRI, which cannot be obtained by conventional DWI methods, and the results indicate close correlation with primary biologic process such as cell death and treatment efficacy such as survival. Data presented in this study provide compelling evidence to justify the further evaluation of IMPULSED in preclinical and clinical applications.

Supplementary data

Supplementary material for this article can be found at https://dx.doi.org/10.1016/j.adro.2018.11.003.

References

1. Eisenhauer EA, Therasse P, Bogaerts J, et al. New response evaluation criteria in solid tumours: Revised RECIST guideline (version 1.1). *Eur J Cancer*. 2009;45:228-247.
2. Schwartz LH, Litiere S, de Vries E, et al. RECIST 1.1-Update and clarification: From the RECIST committee. *Eur J Cancer*. 2016;62: 132-137.
3. Michaelis LC, Ratain MJ. Measuring response in a post-RECIST world: From black and white to shades of grey. *Nat Rev Cancer*. 2006;6:409-414.
4. Chenevert TL, McKeever PE, Ross BD. Monitoring early response of experimental brain tumors to therapy using diffusion magnetic resonance imaging. *Clin Cancer Res*. 1997;3:1457-1466.
5. Mardor Y, Roth Y, Lidar Z, et al. Monitoring response to convection-enhanced taxol delivery in brain tumor patients using diffusion-weighted magnetic resonance imaging. *Cancer Res*. 2001; 61:4971-4973.
6. Thoeny HC, Ross BD. Predicting and monitoring cancer treatment response with diffusion-weighted MRI. *J Magn Reson Imaging*. 2010;32:2-16.
7. Sugahara T, Korogi Y, Kochi M, et al. Usefulness of diffusion-weighted MRI with echo-planar technique in the evaluation of cellularity in gliomas. *J Magn Reson Imag*. 1999;9:53-60.

8. Szafer A, Zhong JH, Gore JC. Theoretical-model for water diffusion in tissues. *Magn Reson Med*. 1995;33:697-712.

9. Xu J, Does MD, Gore JC. Sensitivity of MR diffusion measurements to variations in intracellular structure: Effects of nuclear size. *Magn Reson Med*. 2009;61:828-833.

10. Colvin DC, Jourquin J, Xu J, Does MD, Estrada L, Gore JC. Effects of intracellular organelles on the apparent diffusion coefficient of water molecules in cultured human embryonic kidney cells. *Magn Reson Med*. 2011;65:796-801.

11. Patterson DM, Padhani AR, Collins DJ. Technology insight: Water diffusion MRI—a potential new biomarker of response to cancer therapy. *Nat Clin Pract Oncol*. 2008;5:220-233.

12. Panagiotaki E, Chan RW, Dikaios N, et al. Microstructural characterization of normal and malignant human prostate tissue with vascular, extracellular, and restricted diffusion for cytometry in tumours magnetic resonance imaging. *Invest Radiol*. 2015;50:218-227.

13. Panagiotaki E, Walker-Samuel S, Siow B, et al. Noninvasive quantification of solid tumor microstructure using VERDICT MRI. *Cancer Res*. 2014;74:1902-1912.

14. Jiang X, Li H, Xie J, Zhao P, Gore JC, Xu J. Quantification of cell size using temporal diffusion spectroscopy. *Magn Reson Med*. 2016;75:1076-1085.

15. Xu J, Does MD, Gore JC. Quantitative characterization of tissue microstructure with temporal diffusion spectroscopy. *J Magn Reson*. 2009;200:189-197.

16. Xu J, Li H, Harkins KD, et al. Mapping mean axon diameter and axonal volume fraction by MRI using temporal diffusion spectroscopy. *NeuroImage*. 2014;103C:10-19.

17. Reynaud O, Winters KV, Hoang DM, Wadghiri YZ, Novikov DS, Kim SG. Pulsed and oscillating gradient MRI for assessment of cell size and extracellular space (POMACE) in mouse gliomas. *NMR Biomed*. 2016;29:1350-1363.

18. Xu J, Li K, Smith RA, et al. Characterizing tumor response to chemotherapy at various length scales using temporal diffusion spectroscopy. *PloS One*. 2012;7:e41714.

19. Bongers A, Hau E, Shen H. Short diffusion time diffusion-weighted imaging with oscillating gradient preparation as an early magnetic resonance imaging biomarker for radiation therapy response monitoring in glioblastoma: A preclinical feasibility study. *Int J Radiat Oncol Biol Phys*. 2018;102:1014-1023.

20. Jiang X, Li H, Xie J, Zhao P, Gore JC, Xu J. In vivo imaging of cancer cell size and cellularity using temporal diffusion spectroscopy. *Magn Reson Med*. 2017;78:156-164.

21. Jiang XY, Li H, Zhao P, et al. Early detection of treatment-induced mitotic arrest using temporal diffusion magnetic resonance spectroscopy. *Neoplasia*. 2016;18:387-397.

22. Jiang X, Li H, Zhao P, Manning HC, Gore JC, Xu J. Early detection of treatment-induced apoptosis in tumors using temporal diffusion spectroscopy MRI. *J Nucl Med*. 2015;56:20-48.

23. Gore JC, Xu JZ, Colvin DC, Yankeelov TE, Parsons EC, Does MD. Characterization of tissue structure at varying length scales using temporal diffusion spectroscopy. *NMR Biomed*. 2010;23:745-756.

24. Li H, Jiang X, Xie J, Gore JC, Xu J. Impact of transcytolemmal water exchange on estimates of tissue microstructural properties derived from diffusion MRI. *Magn Reson Med*. 2017;77:2239-2249.

25. Beeman SC, Osei-Owusu P, Duan C, et al. Renal DCE-MRI model selection using bayesian probability theory. *Tomography*. 2015;1:61-68.

26. Le Bihan D, Iima M. Diffusion magnetic resonance imaging: What water tells us about biological tissues. *Plos Biol*. 2015;13:e1002203.

27. Keng PC, Li CK, Wheeler KT. Synchronization of 9L rat brain tumor cells by centrifugal elutriation. *Cell Biophys*. 1980;2:191-206.

28. Hanahan D, Weinberg RA. Hallmarks of cancer: The next generation. *Cell*. 2011;144:646-674.

29. Vaickus LJ, Tambouret RH. Young investigator challenge: The accuracy of the nuclear-to-cytoplasmic ratio estimation among trained morphologists. *Cancer Cytopathol*. 2015;123:524-530.

30. Cohen-Jonathan E, Bernhard EJ, McKenna WG. How does radiation kill cells? *Curr Opin Chem Biol*. 1999;3:77-83.

31. Bedford JS, Mitchell JB, Griggs HG, Bender MA. Radiation-induced cellular reproductive death and chromosome-aberrations. *Radiat Res*. 1978;76:573-586.

32. Kaza N, Kohli L, Roth KA. Autophagy in brain tumors: A new target for therapeutic intervention. *Brain Pathol*. 2012;22:89-98.

33. Campisi J, di Fagagna FD. Cellular senescence: When bad things happen to good cells. *Nat Rev Mol Cell Biol*. 2007;8:729-740.

34. Dewey WC, Ling CC, Meyn RE. Radiation-induced apoptosis: Relevance to radiotherapy. *Int J Radiat Oncol Biol Phys*. 1995;33:781-796.

35. Hendry JH, West CML. Apoptosis and mitotic cell death: Their relative contributions to normal-tissue and tumour radiation response. *Int J Radiat Biol*. 1997;71:709-719.

36. Maier P, Hartmann L, Wenz F, Herskind C. Cellular pathways in response to ionizing radiation and their targetability for tumor radiosensitization. *Int J Mol Sci*. 2016;17.

37. Meyn RE. Apoptosis and response to radiation: Implications for radiation therapy. *Oncology*. 1997;11:349-356. discussion 356, 361, 365.

38. Li H, Chakravarthy AB, Abramson VG, Gore JC, Xu J. *In vivo imaging of mean cell size and density of human breast tumors: A pilot study*. Lisbon, Portugal: ISMRM Workshop on Breaking the Barriers of Diffusion MRI; 2016.

39. Chenevert TL, Stegman LD, Taylor JMG, et al. Diffusion magnetic resonance imaging: An early surrogate marker of therapeutic efficacy in brain tumors. *J Natl Cancer Inst*. 2000;92:2029-2036.

40. Moffat BA, Chenevert TL, Lawrence TS, et al. Functional diffusion map: A noninvasive MRI biomarker for early stratification of clinical brain tumor response. *Proc Natl Acad Sci U S A*. 2005;102:5524-5529.

41. Ryu YJ, Choi SH, Park SJ, Yun TJ, Kim JH, Sohn CH. Glioma: Application of whole-tumor texture analysis of diffusion-weighted imaging for the evaluation of tumor heterogeneity. *PloS One*. 2014;9:e108335.

42. Lambin P, Rios-Velazquez E, Leijenaar R, et al. Radiomics: Extracting more information from medical images using advanced feature analysis. *Eur J Cancer*. 2012;48:441-446.